Structure and magnetism in Dy_xPr_{1-x} and Er_xPr_{1-x} alloys: I. Hexagonal close-packed and Sm structures

2001 J. Phys.: Condens. Matter 13 10175

(http://iopscience.iop.org/0953-8984/13/45/306)

INSTITUTE OF PHYSICS PUBLISHING JOURNAL OF PHYSICS: CONDENSED MATTER

J. Phys.: Condens. Matter **13** (2001) 10175–10189 PII: S0953-8984(01)24947-9

Structure and magnetism in Dy_xPr_{1-x} and Er_xPr_{1-x} alloys: I. Hexagonal close-packed and Sm structures

P S Clegg[1,4], R A Cowley[1], J P Goff[2], D F McMorrow[3], R C C Ward[1] and M R Wells[1]

[1] Oxford Physics, Clarendon Laboratory, Oxford OX1 3PU, UK
[2] Department of Physics, University of Liverpool, Oliver Lodge Laboratory, Liverpool L69 7ZE, UK
[3] Department of Solid State Physics, Risø National Laboratory, Roskilde DK-4000, Denmark

E-mail: clegg@physics.utoronto.ca

Received 15 May 2001
Published 26 October 2001
Online at stacks.iop.org/JPhysCM/13/10175

Abstract

Epitaxial thin films of dysprosium–praseodymium and erbium–praseodymium alloys have been studied using neutron and x-ray diffraction. The magnetic and structural properties have been determined for Dy_xPr_{1-x} for $1.0 \geqslant x \geqslant 0.5$ and for $Er_{0.5}Pr_{0.5}$. The crystal structure is hexagonal close-packed (hcp) for $1.0 \geqslant x \geqslant 0.6$ and changes to the Sm type for $x \sim 0.5$. The hcp samples form basal-plane helices with a transition to ferromagnetism accompanied by a discontinuity in the lattice parameter c. The alloys with the Sm structure form commensurate magnetic structures similar to that of Sm metal with anisotropy dictated by the heavy-rare-earth constituent. The changes in transition temperatures, magnetoelastic effects and modulation wave vector with composition have been studied. The relationships between change in ordering wave vector and magnetization and between transition temperature and the de Gennes factor of the constituents have been established for light–heavy-rare-earth systems.

1. Introduction

The microscopic interactions of the rare-earth metals result in a large variety of measurable phenomena. To understand the nature of the interactions it is essential to study these phenomena in well controlled systems. Alloying a light rare earth with a heavy rare earth creates systems where ions from one end of the period are observed in the crystalline environment which is normal for an ion at the other end of the period. Characterizing such systems presents an

[4] Present address: Department of Physics, University of Toronto, Toronto, Ont. M5S 1A7, Canada.

opportunity to test the model of rare-earth behaviour. Furthermore, alloys of approximately equal proportions have properties unlike those of either of the constituents. Following the whole range of compositions parallels the changes occurring across the rare-earth period. The results presented here concern hcp- and Sm-structure alloys of dysprosium with praseodymium and a Sm-structure alloy of erbium with praseodymium. The results from the dhcp phase are described in the companion paper, reference [1].

Dy is a heavy rare earth; it has the hcp structure and forms a helical magnetic structure below $T_N = 179$ K [2]. The magnetic moments are confined to the basal plane and the wave vector of the helix is along the c-axis. The turn angle between the magnetic moments on successive planes decreases from 43.2° at T_N to 26.5° at $T_C = 89$ K where it drops to zero. Below this temperature a ferromagnetic phase occurs in which the moments are oriented along the $\boldsymbol{a}$-direction in the basal plane. There are associated changes in the lattice parameters. Alloying Dy with Y [3] or Lu [4] is known to suppress the ferromagnetic phase. Merely 5% Y is sufficient to stabilize the helical phase down to 4 K.

Er is also a heavy rare earth with the hcp structure. It has the most complex magnetic phase diagram of the heavy rare earths [5]. Of primary interest here is that, in contrast to Dy, Er has uniaxial anisotropy in a crystal field with hexagonal symmetry.

Pr is a light rare earth, it has the dhcp structure and therefore contains sites of approximately cubic and hexagonal local symmetry. The crystal-field interactions are larger than the exchange and both hexagonal and cubic sites have non-magnetic singlet ground states. Pr does not exhibit spontaneous long-range magnetic order until it is induced by the hyperfine coupling at $T \sim 45$ mK [6]. The hexagonal sites then order to form a longitudinal incommensurate modulation along $\boldsymbol{a}^*$, with antiferromagnetic coupling between adjacent hexagonal layers.

Early experimental work on binary light–heavy-rare-earth alloys is reviewed in reference [6]. Since then there have been a variety of other investigations of the magnetic structures including references [7] and [8]. The hcp alloys have generally been found to have magnetic properties similar to those of the heavy element, while alloys having the Sm structure order in a structure related to the high-temperature ordered structure of Sm metal. The results on Ho_xPr_{1-x} [9] epitaxial hcp alloys show that the low-temperature transitions to structures with ferromagnetic components are suppressed.

In all but the most recent studies the samples were produced using bulk techniques. However, molecular-beam epitaxy now enables the production of precise compositions of alloys that are generally superior to bulk materials in homogeneity and crystalline quality. Epitaxial samples are not identical to perfect bulk materials; in particular the lattice parameters and elastic constants can be altered by the seed layer on which they are grown. This is known as epitaxial strain and the effects on a system are as follows. Firstly, the modifications to lattice parameters created by the seed layer can be large enough to perturb the magnetic behaviour. Secondly, epitaxial registry with the substrate clamps the film, reducing the effect of magnetostrictive forces.

Epitaxial strain is known to modify the behaviour of Dy. The ferromagnetic phase can be suppressed by growing Dy on Y [10] while the Curie temperature can be increased by a factor of two when it is grown on Lu [11]. The basal-plane strains caused by epitaxy are compressive with a Lu seed and expansive with an Y seed. The change in behaviour is qualitatively consistent with expectations for bulk Dy experiencing these strains.

The experimental techniques section, section 2, explains how the samples were grown and characterized. Section 3 describes the magnetic structures obtained from the neutron scattering results and their interpretation. It is divided into two parts according to the crystal structure. The summary, section 4, collates the most important findings.

2. Experimental techniques

The samples were grown using the Balzers 630 facility at the Clarendon Laboratory, Oxford. The Dy alloy samples were grown with a film of Nb forming both the buffer layer and the seed. In its capacity as a buffer the Nb prevented the highly reactive rare-earth metals from coming into contact with the sapphire substrate. As a seed layer the 1250 Å Nb film proved to be ideal for establishing alloy epitaxy. The single-crystal Dy_xPr_{1-x} alloys were then grown with close-to-atomic-plane precision by controlling the substrate temperature and speed of deposition for each element. The substrate was held at 870 °C while the deposition occurred. The Dy was evaporated from a Knudsen effusion cell while the Pr was deposited from an electron-beam source. The combined evaporation rate was 1 Å s^{-1}. The thickness of the alloys was 10 000 Å. A further 250 Å of Nb was deposited on top to form a cap to reduce corrosion. Alloys of composition $x = 1.0, 0.8, 0.7, 0.5$ were grown. The Er alloy sample was grown with a Nb buffer layer and an Y seed. Both the buffer and the seed were grown to thicknesses of 1000 Å. The $Er_{0.5}Pr_{0.5}$ alloy was deposited using the method detailed above.

The crystal structures were determined at room temperature using high-resolution x-ray diffractometers at the Clarendon Laboratory. The x-ray scattering for wave-vector transfer $\boldsymbol{Q}$ along [1 0 q_l] is shown in figure 1. The scattering is determined by the stacking sequence of the close-packed planes. The scattering from $Dy_{0.8}Pr_{0.2}$ and $Dy_{0.5}Pr_{0.5}$ alloys is consistent with that expected for the hcp and Sm crystal structures respectively. Both the $Dy_{0.5}Pr_{0.5}$ and the $Er_{0.5}Pr_{0.5}$ alloys were found to have the nine-plane Sm-type stacking sequence. All the alloys with higher heavy-rare-earth concentrations grew as hcp crystals. Transverse scans through the (002) Bragg peak were used to determine the mosaic spread. The FWHM of the peak indicated values $\sim 0.1^\circ$ which is very reasonable for rare-earth MBE-grown alloys. The widths of the Bragg peaks obtained from scans along [0 0 q_l] indicate plane-spacing coherence

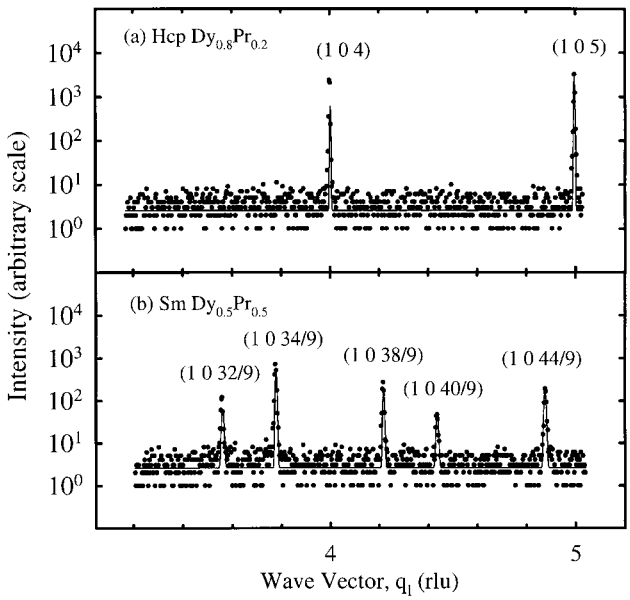

Figure 1. X-ray scattering intensity measured in scans of $\boldsymbol{Q}$ along the [1 0 q_l] for (a) $Dy_{0.8}Pr_{0.2}$ and (b) $Dy_{0.5}Pr_{0.5}$. The peaks are labelled using the hcp reciprocal cell and the crystal structures are (a) hcp and (b) Sm type.

lengths in the growth direction of typically 1300 Å. The plane-ordering coherence length was determined from the FWHM of the Bragg peaks along [1 0 q_l]. For the hcp and Sm structures this was very similar to the plane-spacing coherence length.

Since the crystal structures of the heavy and light rare earths are different it is not possible to verify the sample compositions using the measured lattice parameters and Vegard's law. Previous studies with Ho_xY_{1-x} (where both constituents are hcp) [12] showed that the sample compositions varied by only 2% from the nominal compositions. This is assumed to be the case for these samples as well.

Neutron diffraction studies of the structural and magnetic ordering were carried out using the triple-axis spectrometer TAS1, which is situated on a cold-neutron source at the Risø National Laboratory. Here a fixed incident neutron energy $E_i = 5$ meV was chosen since this gave an adequate range of wave-vector transfer and resolution while allowing the suppression of higher-order scattering with a beryllium filter. The measurements were performed using a variable-temperature cryostat over the range 1.8 K to room temperature and the temperature was controlled to ±0.1 K.

3. Magnetic properties

The crystal structures, Néel temperatures and Curie temperatures determined using neutron scattering techniques are summarized in table 1.

Table 1. Structures and magnetic order in hcp and Sm alloys.

Sample, $\Delta x/x \sim 0.02$	Crystal structure	T_N (T_C) (K) ±2 K	Magnetic structure
Dy film	hcp	184 (85)	Helical (ferromagnetic)
$Dy_{0.8}Pr_{0.2}$	hcp	134 (75)	Helical (ferromagnetic)
$Dy_{0.7}Pr_{0.3}$	hcp	115 (67)	Helical (ferromagnetic)
$Dy_{0.5}Pr_{0.5}$	Sm	73	Sm hexagonal order
$Er_{0.5}Pr_{0.5}$	Sm	17	Sm hexagonal order

3.1. hcp Dy_xPr_{1-x} alloys

The neutron scattering observed from $Dy_{0.7}Pr_{0.3}$ for wave-vector transfers $\boldsymbol{Q}$ along the [0 0 q_l] direction is shown in figure 2 for (a) $T = 30$ K and (b) $T = 70$ K. The magnetic peak in figure 2(b) is displaced from the structural (0 0 2) reflection by an incommensurate modulation vector $\boldsymbol{q}$. The results are consistent with a helical magnetic structure with moments confined to the basal plane and the modulation vector in the $\boldsymbol{c}^*$-direction. At lower temperatures, figure 2(a), the intensity of the Bragg reflection increased and the incommensurate peak vanished, indicating that the sample had become ferromagnetic. This transition was accompanied by a sudden increase in the lattice parameter c. This was measured from the shift in position of the Bragg reflection.

The temperature dependences of the helical modulation vectors for the hcp Dy_xPr_{1-x} alloys are shown in figure 3 with the data for bulk Dy shown for comparison. The behaviour of Dy grown on Nb is similar in this respect to that of bulk Dy. The two hcp alloys show a smaller regime for the helical phase, with the slope of the temperature dependence of the modulation wave vector becoming progressively shallower as the saturated moment decreases. The correlation between the change in wave vector, $\Delta q = (q(T_N) - q(T))$ and the ordered moment, $M(T)$, is illustrated by figure 4. The behaviour is reasonably well described by a

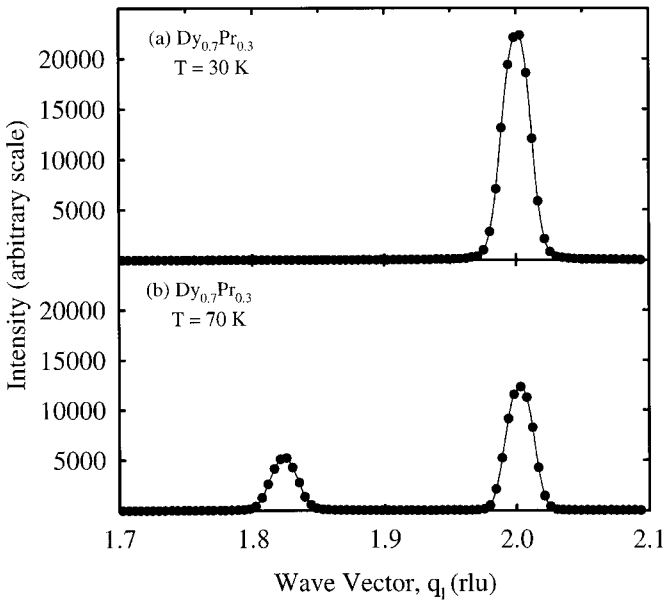

Figure 2. Intensity of neutron scattering from $Dy_{0.7}Pr_{0.3}$ measured in scans of $\boldsymbol{Q}$ along [0 0 q_l] (a) at $T = 30$ K in the ferromagnetic phase and (b) at $T = 70$ K with a peak due to helical magnetic order.

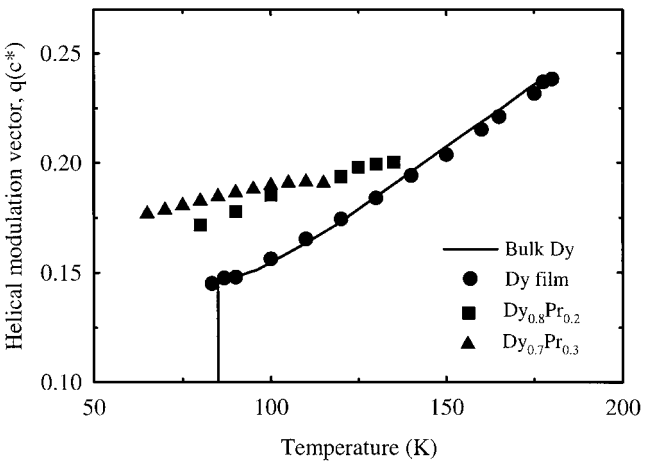

Figure 3. Temperature dependence of the helical modulation wave vector $\boldsymbol{q}$ for hcp Dy_xPr_{1-x} alloys compared with the values for bulk Dy taken from reference [1].

power-law fit, $\Delta q = AM^n$, with $n = 3.4$ for all three films. Very similar behaviour has been observed in Ho and Ho-based alloys [13]. The change in wave vector appears to have the same dependence on the ordered moment whether the moment is varied by temperature or by alloying.

The temperature dependences of the lattice parameters c and b for the hcp alloys and bulk Dy are shown in figure 5. A sharp change occurred in both b and c for the Dy thin film; this corresponds to a change from hcp to orthorhombic symmetry. The c-parameter changes by

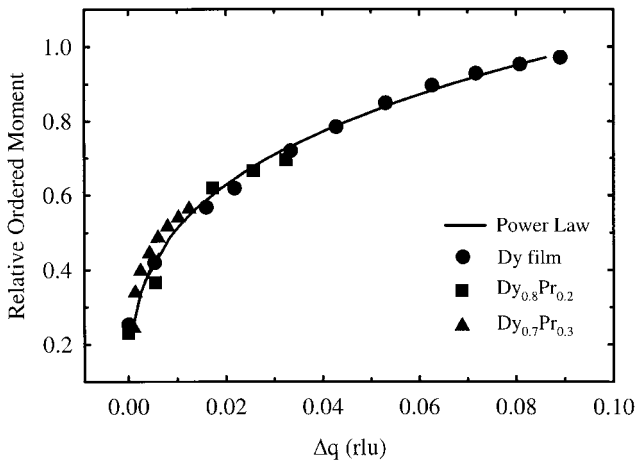

Figure 4. The change in wave vector $\Delta q = (q(T_N) - q(T))$ plotted against the relative ordered moment for hcp Dy_xPr_{1-x} alloys.

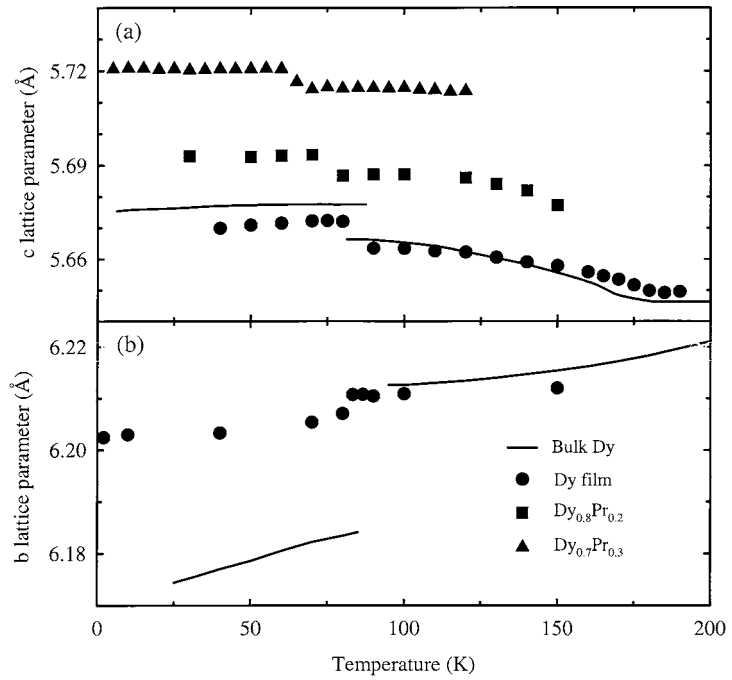

Figure 5. Changes in lattice parameters during the antiferromagnetic-to-ferromagnetic transition: (a) lattice parameter *c* for all hcp samples; (b) lattice parameter *b* for the Dy film only. The measured changes are compared to known values for bulk Dy [14, 15].

a comparable amount to that of the bulk material whereas the change in the *b*-parameter is significantly less; nonetheless it is surprising that such a change in structure can occur in a thin-film epitaxial system. The distortion demonstrates that the epitaxial strain is not strong enough to maintain the hexagonal symmetry. As anticipated for this change in symmetry, the (1 0 0) peak was observed to broaden; see figure 6. The apparent increase in width of the

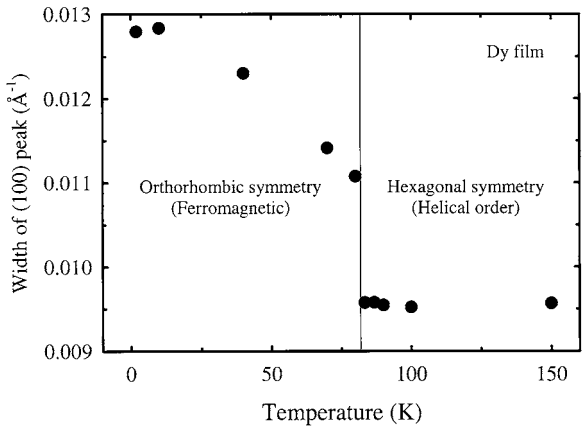

Figure 6. Temperature dependence of the width in q_h of the (1 0 0) peak for hcp Dy film as a result of the transition to orthorhombic symmetry which accompanies the ferromagnetic transition.

peak is interpreted as the effect of the orthorhombic distortion in the three different structural domains. The change in the *b*-parameters for the two hcp alloys was negligible. For these two systems there is still a jump in the *c*-parameter at the ferromagnetic phase transition; however, it is only about 75% of that for the Dy film. This indicates that the role of the magnetoelastic energy in driving the transition is becoming less significant. The change is also apparent in the reduction in the ferromagnetic transition temperatures T_C; see table 1.

The temperature dependences of the intensity of the magnetic peaks for the Dy film and the hcp alloys are shown in figure 7. Instrumental problems led to a loss of alignment with the $Dy_{0.8}Pr_{0.2}$ sample. The helical modulation peaks show a drop in intensity. This has been corrected with reference to the structural scattering intensity. Both measured and corrected data are shown in figure 7; elsewhere only the corrected data are used. The ordered moments on the Dy sites calculated from the measured scattering intensities are shown in table 2. The first set of figures relate to the helical phase; the second set are for the ferromagnetic phase.

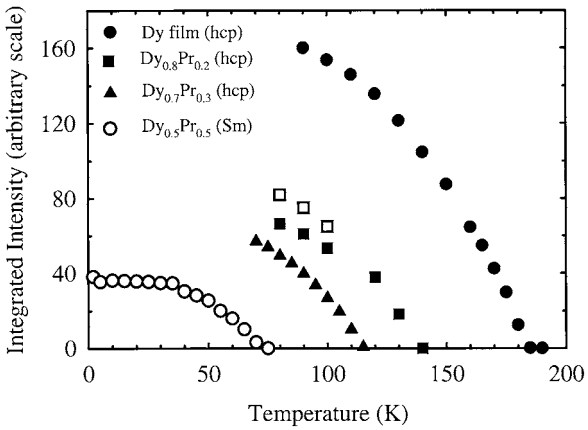

Figure 7. Neutron scattering integrated intensity of the helical (0 0 2 − q) peak for the Dy film and the hcp- and Sm-structure alloys. The open squares show the scattering intensities for the $Dy_{0.8}Pr_{0.2}$ results corrected for a loss of alignment.

Table 2. Ordered moments of Dy sites in Dy_xPr_{1-x} alloys.

x ±0.02	T_{hel} (K) ±0.5 K	μ_1 ±0.5 μ_B	μ_2 ±0.5 μ_B	T_{fm} (K) ±0.5 K	μ_1 ±0.5 μ_B	μ_2 ±0.5 μ_B
1.00	90	5.7	5.7	2	9.1	9.1
0.80	80	5.1	5.5	30	8.4	9.1
0.70	70	4.9	5.7	5	7.8	9.0

The saturated moment was calculated for the alloy from the integrated intensity at the specified temperature. μ_1 is the saturated moment on the Dy sites assuming that only the Dy orders:

$$\mu_1 = \sqrt{\frac{I_M}{I_N}}\frac{\overline{b}}{pF(Q)x} \tag{1}$$

where I_M and I_N are the measured intensities of the magnetic and nuclear scattering respectively, $\overline{b}$ is the average scattering length for this composition, $p = 2.695$ fm is a numerical factor, $F(Q)$ is the magnetic form factor for Dy at the ordering wave vector and x is the concentration of Dy.

Magnetic coupling in the heavy rare earths is dominated by the indirect exchange interaction that couples the spins of the rare-earth ions. Since $\boldsymbol{S}_i = (g_i - 1)\boldsymbol{J}_i$, the relative orientation of spin and total angular momentum changes halfway across the period. This is of importance in the light–heavy-rare-earth alloys since both relative orientations occur. If the spins of both the Dy and the Pr ions are ordered parallel, then the total moments of the two constituents will point in opposite directions. This can be taken into account by subtracting the influence of the Pr moment $(1 - x)[g\boldsymbol{J}]_{\mathrm{Pr}}$ from the Dy moment $x[g\boldsymbol{J}]_{\mathrm{Dy}}$. For this model the unknown is $\mu_2 = [g\boldsymbol{J}]_{\mathrm{Dy}}$:

$$\mu_2 = \sqrt{\frac{I_M}{I_N}}\frac{\overline{b}}{p\overline{F(Q)}(x - (1 - x)R)}. \tag{2}$$

If it is further assumed that the ratios of the moments of the two constituents are the same as the ratios of the gJ-values of the free ions, then $R = [gJ]_{\mathrm{Pr}}/[gJ]_{\mathrm{Dy}} = 3.2\,\mu_B/10\,\mu_B = 0.32$, while $\overline{F(Q)}$ is the average magnetic form factor for this composition.

In table 2, μ_1 designates the Dy moment if only the Dy moments order, while μ_2 is the Dy moment if both the Dy and Pr order. It can be seen that for both the helical and the ferromagnetic order, μ_1 falls with decreasing x. In contrast, μ_2 remains constant as x decreases. This result strongly supports the model in which both the Dy and Pr moments are ordering. It confirms that the spins are being ordered by the indirect exchange and that the total-moment orientation changes as g goes from being less than one to greater than one. This is an essential feature of the magnetic structure of alloys of metals where the two constituents fall either side of a half-filled shell.

At $T = 0$ the Dy moment is expected to be 10 μ_B. Obtaining a moment for Dy, from neutron scattering measurements, that is slightly less than the saturated value is an indiscretion with a good pedigree. Wilkinson *et al* [2] found a saturated moment of 9.5 μ_B while Rhyne *et al* [16] found 9 μ_B for Dy/Y superlattices. The second group of authors were measuring samples which remained in the helical structure down to low temperatures and they were able to integrate an incoherent contribution to the magnetic scattering from a broader region of reciprocal space to reach 10 μ_B. The additional temperature-dependent scattering along the [0 0 q_l] in the present measurement does not make a significant contribution to the moment calculation. Furthermore, calculating the moment from [q_h 0 0] scans through the (1 0 0)

peak does not alter the result. It is possible that the missing moment is spread broadly due to the formation of small ($\leqslant$100 Å) magnetostrictive domains. The measurements made here would have failed to record all of this magnetic scattering. In the recent past, results were presented from ac susceptibility measurements suggesting that Dy has a further phase transition at 6 K [17]. There is the slight possibility that the full moment was not measured because it had ordered in an undocumented structure with a modulation vector in an unanticipated region of reciprocal space.

Amongst the heavy rare-earth elements the transition temperatures are roughly proportional to the de Gennes factor:

$$y = (g-1)^2 J(J+1). \tag{3}$$

This suggests that the height of the peak in the conduction electron susceptibility does not vary strongly. Much use has been made of this factor in analysing the variation of transition temperature with concentration for rare-earth alloys. Koehler [20] and Child *et al* [3] have plotted the transition temperatures of alloys of the heavy rare earths with Y and Lu. For the alloys the de Gennes factor was taken to be the average of the squares of the constituent factors [3]:

$$y = x(g-1)^2 J(J+1). \tag{4}$$

They found universal behaviour of the form $T_N \propto y^{2/3}$ although there is still no explanation of this power law. Bozorth and Suits [21] further extended this work to alloys with two heavy-rare-earth magnetic constituents using

$$y = xy_1 + (1-x)y_2. \tag{5}$$

The two-thirds power law was found again. The factor from equation (5) has been calculated for the hcp- and Sm-structure light–heavy alloys and is plotted against the transition temperature in figure 8. The two-thirds dependence does not yield good agreement for these light–heavy alloys. An approach with a clearer interpretation will be followed here. The average of the squares is not necessarily the most appropriate measure of the de Gennes factor for an alloy. It appears more appropriate to take account of the coupling between each possible pairing of constituents. This method was previously used by Williams [22] in interpreting resistivity measurements on heavy–heavy-rare-earth alloys; here it is adapted for use with light–heavy alloys. The average de Gennes factor can be found for an infinite-range RKKY interaction using

$$\begin{aligned}\mathcal{H} &= -\frac{1}{2}\mathcal{J}\sum_{ij}(g_i-1)(g_j-1)\boldsymbol{J}_i\cdot\boldsymbol{J}_j \\ &= -\frac{1}{2}\mathcal{J}\Bigg(\sum_{i_{\mathrm{A}}j_{\mathrm{A}}}(g_{i_{\mathrm{A}}}-1)(g_{j_{\mathrm{A}}}-1)\boldsymbol{J}_{i_{\mathrm{A}}}\cdot\boldsymbol{J}_{j_{\mathrm{A}}} \\ &\quad + \sum_{i_{\mathrm{B}}j_{\mathrm{B}}}(g_{i_{\mathrm{B}}}-1)(g_{j_{\mathrm{B}}}-1)\boldsymbol{J}_{i_{\mathrm{B}}}\cdot\boldsymbol{J}_{j_{\mathrm{B}}} + \sum_{i_{\mathrm{A}}j_{\mathrm{B}}}(g_{i_{\mathrm{A}}}-1)(g_{j_{\mathrm{B}}}-1)\boldsymbol{J}_{i_{\mathrm{A}}}\cdot\boldsymbol{J}_{j_{\mathrm{B}}}\Bigg).\end{aligned} \tag{6}$$

The first two terms will be related to the de Gennes factor for constituents A and B respectively while the third term is a *cross* de Gennes factor. The dot product can be expanded:

$$2\boldsymbol{J}_{i_{\mathrm{A}}}\cdot\boldsymbol{J}_{j_{\mathrm{B}}} = (\boldsymbol{J}_{\mathrm{A}}+\boldsymbol{J}_{\mathrm{B}})^2 - (\boldsymbol{J}_{\mathrm{A}})^2 - (\boldsymbol{J}_{\mathrm{B}})^2. \tag{7}$$

To evaluate this expression, the details of the two-ion coupling for a light–heavy-rare-earth alloy must be considered. The indirect exchange interaction couples the spins of the ions via the polarization of the conduction electrons. Since the total angular momentum $\boldsymbol{J}$ is a constant of the motion, the moments are most usefully expressed as $\boldsymbol{S} = (g-1)\boldsymbol{J}$. If A and B are ions

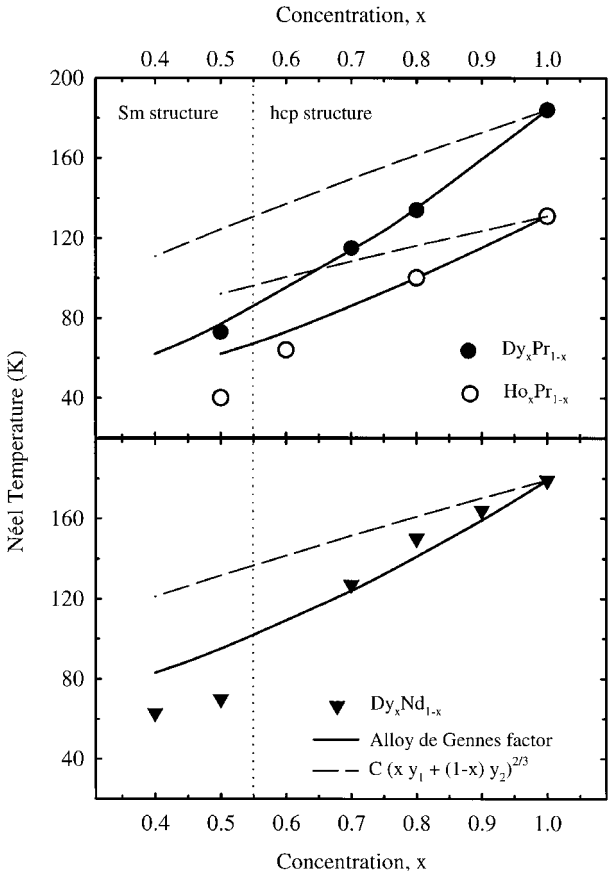

Figure 8. The variation of the Néel temperature with alloy composition; the upper panel is for Dy_xPr_{1-x} and Ho_xPr_{1-x} [9], while the lower panel is for Dy_xNd_{1-x} [19]. The two lines are model results; the solid line is T_N if it is proportional to the *alloy de Gennes factor*, while the dashed line is T_N if it is proportional to a combination of the constituent de Gennes factors to the 2/3 power.

from opposite ends of the period, then the values of g for the two constituents will fall either side of one. This implies that the two total moments will be aligned antiparallel. Equation (7) can be evaluated in line with this:

$$2\boldsymbol{J}_{i_A} \cdot \boldsymbol{J}_{j_B} = (J_A - J_B)(J_A - J_B + 1) - J_A(J_A + 1) + J_B(-J_B + 1) \tag{8}$$

$$= -2J_A J_B. \tag{9}$$

The *cross* de Gennes factor is

$$y_{AB} = -(g_A - 1)(g_B - 1)J_A J_B. \tag{10}$$

Performing the averages of the sums in equation (6) the transition temperature is found to depend on concentration in the following manner:

$$T_N \propto x^2 y_A + (1 - x)^2 y_B + 2x(1 - x)y_{AB}. \tag{11}$$

Figure 8 shows a plot of transition temperature against the *alloy de Gennes factor* for three alloys. In the top panel Dy_xPr_{1-x} and Ho_xPr_{1-x} [9] are shown, while in the bottom panel the results for Dy_xNd_{1-x} appear [19]. In all cases the model describes the data well in the

hcp range. There is a significant departure from this relationship as the Sm-structure region is approached. The magnetic behaviour for the Sm-structure samples is considerably different, so the departure from the model is not a surprise. The linear dependence of the transition temperature on the *alloy de Gennes factor* in the hcp concentration range indicates that the alloys have similar conduction electron susceptibilities. This is a more satisfactory conclusion than a mysterious power law.

3.2. Sm-structure alloys

Two samples had the Sm crystal structure: $Dy_{0.5}Pr_{0.5}$ and $Er_{0.5}Pr_{0.5}$. With both samples, magnetic peaks were detected at (1 0 1/9), (1 0 5/9) and (1 0 7/9) using the hcp basis for reciprocal space. The Dy alloy had a magnetic reflection at (0 0 5/3). The ordering wave vectors are independent of temperature and the peak intensities increase steadily with decreasing temperature until saturation occurs (see figure 7 for $Dy_{0.5}Pr_{0.5}$). The neutron scattering from the Sm-structure alloys is shown in figure 9 for scans of $\boldsymbol{Q}$ along [0 0 q_l] ((a) and (b)) and [1 0 q_l] ((c) and (d)). For both samples the observed magnetic reflections are consistent with a magnetic structure comprising ferromagnetic planes in the sequence $0++0--0++0--0++0--$ similar to that observed in Sm metal [23]. The presence of the (0 0 5/3) reflection for $Dy_{0.5}Pr_{0.5}$ and its absence for $Er_{0.5}Pr_{0.5}$ indicates that the moment directions are different for these two systems. The Er alloy, in common with elemental Sm, has an ordered moment which is directed along the c-axis. By contrast, the Dy alloy has a moment which is confined in the basal plane. This has been observed previously for Ho_xPr_{1-x} alloys with the Sm crystal structure [9]. The differing anisotropies indicate that the heavy-rare-earth moments on the hexagonal symmetry sites are experiencing a similar crystal field to those in the hcp crystal structure. The Er and Dy moments have the same anisotropies, uniaxial and easy planar respectively, as they have as hcp elements.

A difference between these two alloys and Sm metal is that in the latter there is an additional low-temperature transition in which the cubic sites order. This final transition is suppressed in the alloys. The magnetic moments in table 3 were calculated using equations (1) and (2) and the assumption was made, consistent with the experimental results, that the moments were ordered on only the hexagonal symmetry sites. The saturated moment of Er is 9 μ_B while that of Dy is 10 μ_B. The μ^{bp}-results for the $Dy_{0.5}Pr_{0.5}$ alloy indicate the Pr moments order antiparallel to the Dy moments (table 3). The situation with the $Er_{0.5}Pr_{0.5}$ alloy requires more careful consideration. The absence of a magnetic reflection in figure 9(b) demonstrates unambiguously that the Pr moments are not ordering in the basal plane. Two other possibilities remain: firstly, that Pr adopts a singlet ground-state configuration or, secondly, that it is ordered and is aligned antiparallel to the Er moments. If the Pr moments were not ordered, then the Er moments at 2 K would have the value μ_1^c shown in table 3, whereas if the Er and the Pr moments were combined in the ratio of the saturated moments, then the Er moment would be μ_2^c. These values were calculated using equations (1) and (2) respectively. Since the saturated

Table 3. Saturated moments of heavy sites in Sm-structure alloys.

Sample	T_{hel} (K) ±0.5 K	μ_1^c ±0.5 μ_B	μ_2^c ±0.5 μ_B	μ_1^{bp} ±0.5 μ_B	μ_2^{bp} ±0.5 μ_B
$Dy_{0.5}Pr_{0.5}$	2	0.0	0.0	7.1	10.4
$Er_{0.5}Pr_{0.5}$	2	6.5	10.1	0.0	0.0

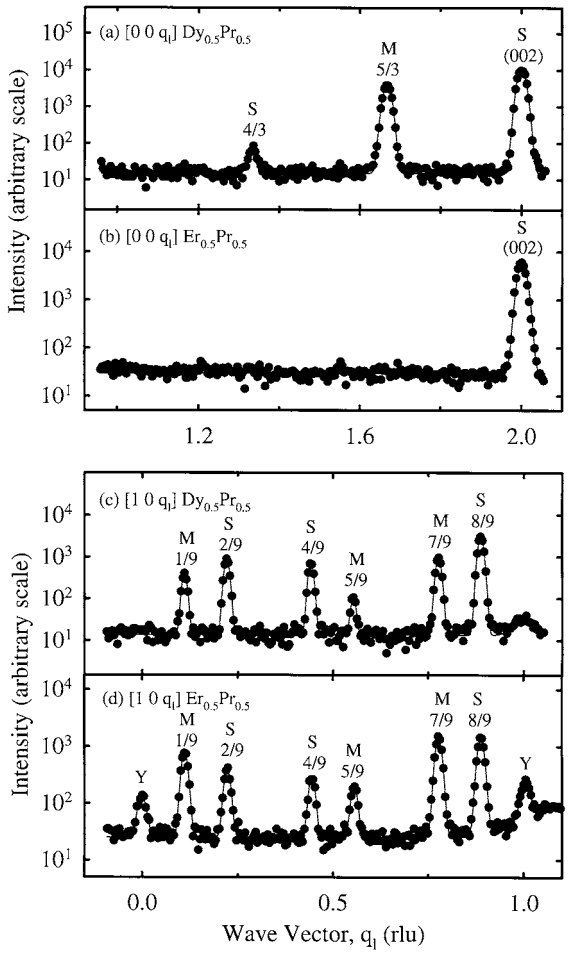

Figure 9. Neutron scattering intensity measured in scans of $\boldsymbol{Q}$ along (a) [0 0 q_l] and (c) [1 0 q_l] for $Dy_{0.5}Pr_{0.5}$ and (b) [0 0 q_l] and (d) [1 0 q_l] for $Er_{0.5}Pr_{0.5}$ with both samples at 2 K. The structural and magnetic peaks are labelled S and M, respectively. The fractions give q_l in units of c^* using the hcp reciprocal cell.

moment for Er is 9 μ_B, the values in table 3 suggest that there is likely to be a moment on the Pr sites aligned antiparallel to the Er moments.

The Néel temperatures observed for these two systems are very different (table 1). Considering that the moments and the concentrations are similar, this might initially appear surprising. Figure 10 shows the Néel temperature plotted against the average de Gennes factor (see equation (11)) for Sm and another epitaxial Pr–heavy-rare-earth alloy with Sm structure (from reference [8]). To a reasonable approximation, the alloys all appear to fall on the same straight line. The Sm transition temperature is significantly lower than would be expected for a Pr–heavy-rare-earth alloy with the same de Gennes factor. For the alloys the linear dependence of the transition temperature on the de Gennes factor suggests that in this crystal structure the conduction electron susceptibility is roughly independent of the particular constituents. The observed relationship predicts that the transition temperature will go to zero while the de Gennes factor is still finite. This suggests that the conduction electron susceptibility of the

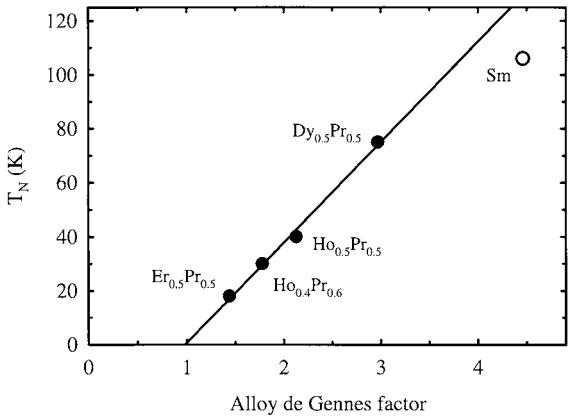

Figure 10. Transition temperature as a function of the average de Gennes factor for a series of MBE-grown Sm-structure alloys of Pr. The straight line shows the dependence of T_N on the product of the spin contributions to the moments.

Pr–heavy-rare-earth alloys hinders ordering via the indirect exchange interaction with this wave vector for small moments. Since the magnetic structures of the light rare-earth metals are very different to those of Sm or the heavy rare earths, this does not seem unreasonable.

4. Summary

A series of epitaxial light–heavy-rare-earth alloys have been studied using x-ray diffraction and neutron scattering techniques. The hcp Dy_xPr_{1-x} alloys form helical magnetic structures followed by a transition to basal-plane ferromagnetic order. Calculations of the ordered moment indicate that both the Dy and the Pr moments order and that they are aligned anti-parallel. The measurements show that the magnetoelastic effects are surprisingly robust. In contrast to Dy_xLu_{1-x} [4], Dy_xY_{1-x} [3] and Ho_xPr_{1-x} [9] the hcp alloys continue to exhibit a ferromagnetic component to the ordered moment at low temperatures. The transition continues to be associated with magnetoelastic changes, although the importance of this contribution diminishes with decreasing Dy concentration.

The observed magnetic structures in the hcp Dy_xPr_{1-x} alloys are similar to those of Dy metal. This suggests that the various interactions are not changing very quickly with alloy composition in this regime. The transition temperatures have been related to an appropriate alloy average of the de Gennes factor with good agreement. This indicates that the conduction electron susceptibility is only changing slowly with x. There is a small drop in transition temperature, compared to the alloy de Gennes factor model, as the crystal structure goes from hcp to Sm-type. This is expected since the band structure is changing and in addition only two thirds of the planes order in the Sm-structure light–heavy alloys. The transition temperatures of the Sm-structure alloys have been shown to vary linearly with the alloy average de Gennes factor. Hence Sm-structure light–heavy-rare-earth alloys appear to have similar conduction electron susceptibilities (figure 10).

The magnetization dependence of the ordering wave vector for the Dy film and hcp alloys shows very similar behaviour to that observed in Ho_xY_{1-x} [12], Ho_xLu_{1-x} [13] and Ho_xSc_{1-x} [18] alloys. The temperature dependence of the modulation wave vector is much weaker in the dilute alloys than it is in more concentrated systems due to the decrease in the ordered moment. $\Delta q = (q(T_N) - q(T))$ is proportional to magnetization to the power of 3.4

which is similar to the case for Ho alloys [13]. Alloying and changes in temperature alter the magnetization and give rise to the same change in the ordering wave vector. Both changes are likely to be due to the effect of the ordered moment on the band structure, although the reason for the particular value of the exponent is not understood.

The two alloys with an equal balance of light and heavy rare earths: $Dy_{0.5}Pr_{0.5}$ and $Er_{0.5}Pr_{0.5}$ grew in the Sm-type crystal structure. The magnetic structures formed in the two alloys were similar, while the transition temperatures were significantly different. The magnetic structure was on the hexagonal symmetry sites and with Dy ions exhibiting basal-plane anisotropy and Er uniaxial anisotropy. The intensity of the magnetic scattering is consistent with both the heavy- and light-rare-earth moments being ordered but aligned antiparallel. Table 4 shows the crystal-field parameters for Pr, Dy and Er as pure metals. Since B_2^0 is positive for both Dy and Pr, this Sm-type alloy is an easy-planar system. The value of B_2^0 for Pr is almost double that for Dy, indicating that the planar anisotropy is very strong. The situation is different for Er, where B_2^0 is seen to be negative. This means that the Er moment will prefer to align along the *c*-axis on the hexagonal symmetry planes. In the $Er_{0.5}Pr_{0.5}$ alloy the moment is found to be aligned along the *c*-axis. In addition, the results suggest that the Pr moments on the hexagonal planes have ordered pointing along the *c*-axis. This is a surprising result, since Pr is strongly easy planar. It is widely believed [24] that the anisotropy in Pr is dominated by a two-ion effect. The origins of this coupling are not known. It is possible that by disrupting the anisotropic two-ion coupling, the Er moments have altered the anisotropy.

Table 4. Crystal-field parameters in meV.

Ion^{3+}	B_2^0	B_4^0	B_6^0	B_6^6
Pr	0.19	-5.7×10^{-4}	10×10^{-5}	-96×10^{-5}
Dy	0.11	-1.3×10^{-4}	0.14×10^{-5}	1.3×10^{-5}
Er	−0.027	-0.3×10^{-4}	0.13×10^{-5}	-0.19×10^{-5}

Acknowledgments

The expert technical assistance of the staff at Risø National Laboratory is gratefully acknowledged. Financial support was provided by the EPSRC in the UK and by the EU under its Large Installation Programme in Denmark.

References

[1] Clegg P S, Cowley R A, Goff J P, McMorrow D F, Sawicki M, Ward R C C and Wells M R 2001 *J. Phys.: Condens. Matter* **13** 10191–206
[2] Wilkinson M K, Koehler W C, Wollan E O and Cable J W 1961 *J. Appl. Phys.* **32** 48S–9S
[3] Child H R, Koehler W C, Wollan E O and Cable J W 1965 *Phys. Rev.* **138** A1655–60
[4] Everitt B A, Salamon M B, Flynn C P, Park B J, Borchers J A, Erwin R W and Tsui F 1994 *J. Appl. Phys.* **75** 6592–4
[5] Habenschuss M, Stassis C, Sinha S K, Deckman H W and Spedding F H 1974 *Phys. Rev.* B **10** 1020–6
[6] Bjerrum Møller H, Jensen J Z, Wulff M, Mackintosh A R, Masters O D and Gschneidner K 1982 *Phys. Rev. Lett.* **49** 482–5
[7] Coles B R 1984 *J. Less-Common Met.* **100** 93–103
[8] Kawano S 1989 *J. Phys. Chem. Solids* **50** 633–9
[9] Goff J P, Bryn-Jacobsen C, McMorrow D F, McIntyre G J, Simpson J A, Ward R C C and Wells M R 1998 *Phys. Rev.* B **57** 5933–40

[10] Dumesnil K, Dufour C, Marchal G, Mangin Ph and Hennion M 1995 *Europhys. Lett.* **31** 43–8
[11] Beach R S, Borchers J A, Matheny A, Erwin R W, Salamon M B, Everitt B, Petit K, Rhyne J J and Flynn C P 1993 *Phys. Rev. Lett.* **70** 3502–5
[12] Cowley R A, Ward R C C, Wells M R, Matsuda M and Sternlieb B 1994 *J. Phys.: Condens. Matter* **6** 2985–98
[13] Swaddling P P, Cowley R A, Ward R C C, Wells M R and McMorrow D F 1996 *Phys. Rev.* B **53** 6488–98
[14] Darnell F J 1963 *Phys. Rev.* **130** 1825–8
[15] Darnell F J and Moore E P 1963 *J. Appl. Phys.* **34** 1337–8
[16] Rhyne J J, Erwin R W, Borchers J A, Salamon M B, Du R and Flynn C P 1989 *J. Less-Common Met.* **148** 17–33
[17] Willis F and Ali N 1991 *J. Appl. Phys.* **70** 6548–9
[18] Bryn-Jacobsen C, Cowley R A, McMorrow D F, Goff J P, Ward R C C and Wells M R 1997 *Phys. Rev.* B **55** 317–29
[19] Chatterjee D and Taylor K N R 1972 *J. Phys. F: Met. Phys.* **2** 151–8
[20] Koehler W C 1965 *J. Appl. Phys.* **36** 1078–87
[21] Bozorth R M and Suits J C 1964 *J. Appl. Phys.* **35** 1039–40
[22] Williams D E G 1973 *J. Phys. F: Met. Phys.* **3** 1898–902
[23] Koehler W C and Moon R M 1972 *Phys. Rev. Lett.* **29** 1468–72
[24] Jensen J and Mackintosh A R 1991 *Rare Earth Magnetism—Structures and Excitations* (New York: Oxford Science)